Thin Solid Films 592 (2015) 59–68

Contents lists available at ScienceDirect

Thin Solid Films

journal homepage: www.elsevier.com/locate/tsf

Structure and composition effects on electrical and optical properties of sputtered PbSe thin films

Xigui Sun [a], Kewei Gao [a], Xiaolu Pang [a,*], Huisheng Yang [a], Alex A. Volinsky [b]

[a] Department of Materials Physics and Chemistry, University of Science and Technology Beijing, Beijing 100083, China
[b] Department of Mechanical Engineering, University of South Florida, Tampa, FL 33620, USA

ARTICLE INFO

Article history:
Received 8 October 2014
Received in revised form 29 August 2015
Accepted 3 September 2015
Available online 5 September 2015

Keywords:
Magnetron sputtering
Lead selenide
Thin films
Photoelectric properties
Optical properties

ABSTRACT

Lead selenide (PbSe) thin films were grown on Si (111) substrates using magnetron sputtering, and the structure and composition effects on the photoelectric and optical properties of the sputtered PbSe thin films were studied using field emission scanning electron microscope, energy dispersive X-ray detector, X-ray diffraction, X-ray photoelectron spectroscopy, physical property measurement system and Fourier transform infrared spectroscopy. The optical band gaps of all the sputtered PbSe thin films ranged from 0.264 eV to 0.278 eV. The PbSe thin film prepared with oxygen flux 1.0 sccm, deposition time 240 min, sputtering power 150 W and substrate temperature 150 °C showed the highest resistance change rate under illumination, about 84.47%. The variation trends of the photoelectric and optical properties with the average crystal size, lattice constant, oxygen content and lattice oxygen percentage were similar, respectively. The sputtered PbSe thin films showed poor photoelectric sensitivity, when the average crystal size was similar to the Bohr radius (46 nm), while the photoelectric sensitivity increased almost linearly with the oxygen content in the thin films, indicating that both deviating the average crystal size from the Bohr radius and increasing the oxygen content are two direct and effective ways to obtain high photoelectric sensitivity in PbSe thin films.

1. Introduction

In 1874 Ferdinand Braun was the first to report electrical rectification with natural galena (lead sulfide, PbS) [1]. From then on, lead chalcogenides (PbS, PbTe and PbSe) and their alloys (PbSeTe, PbSnSe, PbSnTe and PbSnSeTe) were widely used as semiconductor devices, such as light emitting diodes [2], laser diodes [3], infrared photodetectors [4], solar cells [5] and thermoelectric devices [6], due to their excellent photoelectric and thermoelectric properties.

Lead chalcogenides are typical narrow band gap materials (0 eV to 0.5 eV), leading to a remarkable spectrum absorption range from 3 μm to 30 μm for the lead chalcogenide devices [7]. On the other hand, the high permittivity of lead chalcogenides can effectively shield the charge carriers from the lattice defects, yielding superior fault-tolerant properties [8].

Compared with other lead chalcogenide materials, lead selenide (PbSe) has the largest exciton Bohr radius of about 46 nm and a relatively small effective mass of the exited electron–hole pair, which allows remarkable quantum confinement in large crystals [9]. In addition, the PbSe infrared detectors can maintain excellent detective ability in the mid-wavelength infrared range, even at room temperature, which leads to a great interest in the fundamental studies of this material and its alloys [10–14].

The deposition of the PbSe thin films has been carried out by a variety of chemical and physical deposition techniques, such as chemical bath deposition [15], electrochemical deposition [16], thermal evaporation [17], atomic layer deposition [18], molecular beam epitaxy [19], sputter deposition [20] and several other improved methods [21–23]. In the present work, the magnetron sputtering technique was used to deposit the PbSe thin films due to its medium cost, easy handling, high quality products and the potential for mass production, compared with other methods. Moreover, multiple deposition parameters, such as the gas flux, sputtering power, distance between the target and the substrate, substrate temperature, deposition time and so on, can be varied to modify the physical and chemical properties of the sputtered PbSe thin films, which in turn affect the performance of the PbSe devices. Within this research, two parameters, oxygen flux and deposition time, were varied in order to prepare the different composition and structure PbSe thin films, while other parameters remained the same, based on the previous experiments.

The photoelectric and optical properties of the PbSe thin films are affected by several factors, including the film thickness, composition, and crystal structure. Barote et al. [24] found that the average crystal size, bang gap, carrier mobility and concentration of the chemical bath

* Corresponding author.
E-mail address: pangxl@mater.ustb.edu.cn (X. Pang).

http://dx.doi.org/10.1016/j.tsf.2015.09.009
0040-6090/

deposited PbSe thin films all increased with the film thickness. On the other hand, Jung et al. [20] demonstrated that the oxidized surface of the radio frequency magnetron sputtered PbSe nanowires significantly influenced their optical properties and produced strong confined states. Moreover, Gautier et al. [25] found that the oxygen-induced sensitization in the polycrystalline PbSe could alter the microstructure, phase composition, and other material properties. However, most of the previous reports dealt with the sensitization treatment after the deposition of the PbSe materials, while the influence of the oxygen sensitization treatment during the preparation of the PbSe thin films has not been studied in detail yet.

In the present work, the PbSe thin films with different composition and structure were deposited on Si (111) substrates using magnetron sputtering technique with different deposition parameters. In order to identify the optimistic deposition parameters, the relationships between the composition, crystal structure, surface composition, photoelectric and optical properties of the sputtered PbSe thin films were studied using the field emission scanning electron microscopy (FE-SEM), energy dispersive X-ray spectroscopy (EDX), X-ray powder diffraction (XRD), X-ray photoelectron spectroscopy (XPS), Fourier transform infrared spectroscopy (FT-IR) and the physical properties measurement system (PPMS). Moreover, the effects of the structure (mainly average crystal size and lattice constant) and composition (mainly oxygen content and lattice oxygen percentage) of the sputtered PbSe thin films on the photoelectric and optical properties of the sputtered PbSe thin films were studied in detail, which provides guiding significance for the preparation of high quality PbSe thin films.

2. Experiment

2.1. Deposition equipment

PM500-S sputtering system equipped with the MF-5K medium frequency sputtering power source was used to deposit the PbSe thin films. The PbSe alloy targets were prepared by conventional powder metallurgy with the composition of n_{Pb}:n_{Se} = 45:55 (99.99% purity), based on the easier deposition of the Pb element than the Se element due to the high volatility of the Se element and different condensation coefficients for these two elements. The single-side polished Si (111) wafers with 15 × 10 × 0.5 mm^3 dimensions were chosen as the substrates. Prior to being fixed to the substrate holder, these Si substrates were ultrasonically washed in deionized water, ethanol and acetone for 15 min, respectively.

2.2. PbSe thin films deposition

The PbSe thin films were grown on the Si (111) substrates by the magnetron sputtering with different deposition parameters under 5×10^{-3} Pa base pressure. During the whole sputtering process, two different oxygen fluxes and three deposition times were used to prepare the PbSe thin films while other sputtering parameters remained the same, as listed in Table 1. Moreover, the argon flux was set to 30 sccm during the ion bombarding and magnetron sputtering process.

Table 1
Sputtering process parameters for the PbSe thin films.

Sample	Oxygen flux (sccm)	Time (min)	Sputtering power (W)	Substrate temperature (°C)
PbSe1	0.5	120	150	150
PbSe2	0.5	180	150	150
PbSe3	0.5	240	150	150
PbSe4	1.0	120	150	150
PbSe5	1.0	180	150	150
PbSe6	1.0	240	150	150

According to the previous research, the film thickness significantly affects the average crystal size and the lattice constant, which in turn affects the photoelectric and optical properties of the PbSe thin films [26]. In the present work, the deposition time was set to 120 min, 180 min, and 240 min, respectively.

The film surface oxidation technique during (or after) the deposition process, also known as "sensitization", is essential to obtain remarkable photoelectric and optical properties in the PbSe thin films. Within this process, oxygen atoms act as acceptors, causing the appearance of the p-type charge carriers, whose presence can radically change the physicochemical properties of the thin films [27]. In addition, the oxygen atoms can create impurity levels in the forbidden band of the PbSe thin films, which can increase the density of states, and subsequently increase the charge carrier concentration during the activation process, such as illumination [28]. However, oxygen can react with the PbSe target, and the products will cover the target surface and create excess positive charges, which will increase the target surface positive potential and decrease the cathode dark space negative potential, and when the cathode dark space negative potential reaches zero, the sputtering process will be ceased. This process is also known as target poisoning [29]. Thus, the oxygen flux was set to less than 1 sccm, based on the previous research results.

2.3. PbSe property characterization

The field emission scanning electron microscope (FE-SEM, Zeiss Auriga) with 15 kV operating voltage was used to study the surface and cross-section morphology of the sputtered PbSe thin films.

The photoelectric properties of the sputtered PbSe thin films were characterized by the resistance change rate under certain illumination. The resistance of the films was recorded in the dark for 300 s and under illumination (using a 275 W infrared light source) for another 300 s with a step of 20 s. The resistance change rate under illumination, labeled as $\Delta\tilde{R}_t$, was calculated as follows:

$$\Delta\tilde{R}_t = \frac{R_D - R_{Lt}}{R_D} \times 100\% \quad (1)$$

where R_D represents the average value of the dark resistance recorded before the illumination treatment and R_{Lt} is the value of the light resistance of the sputtered thin films at the illumination time t. The dc electrical resistance of the sputtered PbSe thin films was measured using the four-probe method as a function of the film temperature from 25 °C to 100 °C using the physical properties measurement system (PPMS, Quantum Design, Inc., USA). A quick drying silver paste was used to bond the electrode line in order to decrease the ohmic contact.

The XRD studies were performed on the rotating anode diffractometer (Dmax-RB 12 kW, Rigaku, Japan) with the Cu radiation source, λ = 1.5406 Å. These measurements were undertaken at a scan rate of 8°/min for the 2θ scanning angle ranging from 10° to 65°.

The surface composition of the sputtered PbSe thin films was analyzed by the X-ray photoelectron spectroscopy (XPS) measurements performed using the AXIS ULTRA^{DLD} (Shimadzu, Japan) X-ray photoelectron spectrometer equipped with the Al Kα source, $h\nu$ = 1486.6 eV. The operating voltage and power were 12 kV and 200 W, respectively, and the vacuum was 1×10^{-7} Pa. In order to study the thickness of the oxide layer and the difference of chemical states on and beneath the film surface, additional XPS analysis was performed on the PbSe6 sample after the film surface was etched for 60 s by Ar^+ with the etching energy of 3000 eV. The Ar^+ etching and XPS analysis cycle was conducted eleven times.

The optical properties of the sputtered PbSe thin films were studied using the infrared absorption spectra recorded on the Nicolet Nexus 470 Fourier transform infrared spectrometer (FT-IR) ranging from 4000 cm^{-1} to 400 cm^{-1} at room temperature.

3. Results and discussion

3.1. Film surface and cross-section morphology

The surface properties, such as roughness, impurities and defects, significantly affect the performance of the PbSe thin film devices, especially their lifetime. Fig. 1 presents the surface and the cross-section (inset) morphology of the sputtered PbSe thin films, which are quite smooth and compact, indicating that magnetron sputtering is a quite competitive method to prepare the PbSe thin films. Moreover, the surface of the PbSe thin films prepared under 0.5 sccm oxygen flux (PbSe1, PbSe2 and PbSe3) is smoother than the films prepared under 1 sccm oxygen flux (PbSe4, PbSe5 and PbSe6), confirmed by the roughness results obtained using the profilometer, as listed in Table 2. The difference may be attributed to the different growth rates under different oxygen fluxes.

The thickness of the sputtered PbSe thin films is about 1000 nm for PbSe1 and PbSe4, 1400 nm for PbSe2 and PbSe5, and 1800 nm for PbSe3 and PbSe6, according to the cross-section images, and the results are listed in Table 2. The film thickness is mainly affected by the deposition time, and the average deposition rate is about 7.57 nm/min and 8.25 nm/min for the sputtered PbSe thin films deposited under 0.5 sccm and 1 sccm oxygen flux, respectively.

3.2. Photoelectric properties

As mentioned above, $\Delta\tilde{R}_t$ of the sputtered PbSe thin films is a useful parameter to evaluate their photoelectric properties. Fig. 2(a) shows the resistance values of PbSe1 in the dark and under certain illumination. Other five PbSe thin films show a similar variation trend and the data are not shown in this paper. The film resistance remains almost constant in the dark and decreases sharply as the light turns on, however, the rate of decrease gets lower after 20 s of illumination. Moreover, the resistance wasn't saturated during 300 s, which may be attributed to the long lifetime of the free charge carriers due to the existence of the deep localized gap states generated by the oxide impurities.

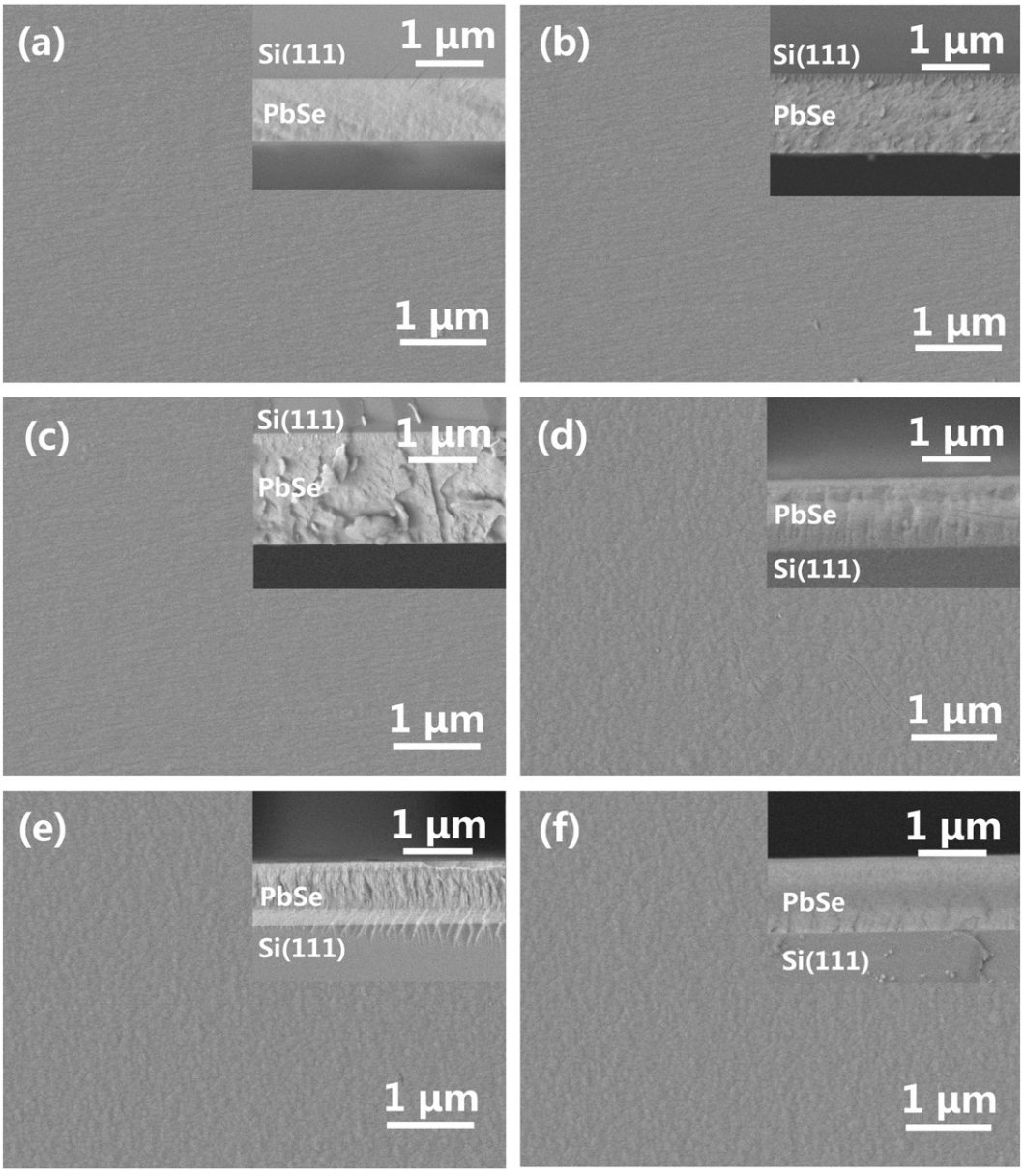

Fig. 1. FE-SEM images of the surface and cross-section (inset) morphology of the sputtered PbSe thin films prepared under different oxygen flux and deposition time: (a) PbSe1; (b) PbSe2; (c) PbSe3; (d) PbSe4; (e) PbSe5; (f) PbSe6.

Table 2
Thickness, roughness, photoelectric and optical properties of the sputtered PbSe thin films.

Sample	Thickness (nm)	Roughness (nm)	R_D (KΩ)	R_L (20–300 s) (KΩ)	$\Delta\tilde{R}^a$ (%)	ΔE_a (eV)	E_g (eV)
PbSe1	1023	5.5 ± 0.3	17.56 ± 0.04	8.13–5.12	64.01	0.171	0.264
PbSe2	1231	6.0 ± 0.3	118.51 ± 0.09	40.24–26.05	74.70	0.209	0.275
PbSe3	1781	5.8 ± 0.4	16.45 ± 0.02	7.87–4.95	64.65	0.153	0.271
PbSe4	1066	12.0 ± 0.9	36.18 ± 0.05	12.13–9.92	71.07	0.141	0.273
PbSe5	1501	33.9 ± 2.1	123.71 ± 0.08	47.40–29.59	71.47	0.104	0.273
PbSe6	1810	24.1 ± 1.5	64.52 ± 0.07	12.94–9.20	84.47	0.096	0.278

[a] The resistance change rate under illumination $\Delta\tilde{R}$ is the average value from 20 s to 300 s under illumination, i.e., $\Delta\tilde{R} = \frac{\Delta\tilde{R}_{20}+\Delta\tilde{R}_{40}+\cdots\cdots+\Delta\tilde{R}_{300}}{15}$.

The $\Delta\tilde{R}_t$ values at different illumination time were calculated using the Eq. (1), and the results are shown in Fig. 2(b). The average value of $\Delta\tilde{R}$ from 20 s to 300 s was calculated to evaluate the photoelectric sensitivity of the sputtered PbSe thin films, as listed in Table 2. PbSe6 shows the highest $\Delta\tilde{R}$ compared with the other five samples, indicating that the optimal deposition parameters to prepare high photoelectric sensitivity PbSe thin films were: oxygen flux 1.0 sccm, deposition time 240 min, sputtering power 150 W and substrate temperature 150 °C.

The electrical resistivity, ρ, of the sputtered PbSe thin films reveals important and reliable information about the transport phenomenon of the materials, which was measured in the 25 °C to 100 °C temperature range using the four-probe method, as shown in Fig. 3(a). The resistivity of the sputtered PbSe thin films shows negative temperature dependence, indicating their semiconducting nature. Moreover, the plots consist of the two distinct linear regions separated at about 50 °C, indicating the presence of two conduction mechanisms [30]. The extrinsic conductive mechanism in the low temperature region (25 °C to 50 °C) is attributed to the transition of the charge carriers between the impurity energy levels and conduction band energy levels. In order to identify the conduction mechanism during the high temperature region (about 50 °C to 100 °C), the activation energy ΔE_a was calculated using the following equation, based on Fig. 3(b):

$$\sigma_{dc} = \sigma_0 \exp(-\Delta E_a / kT) \quad (2)$$

where σ_{dc} is the conductivity of the PbSe samples, which can be directly obtained from the resistivity of the samples shown in Fig. 3(a), σ_0 is a constant, k is the Boltzmann constant and T is the temperature in K. As listed in Table 2, the activation energy of the sputtered PbSe thin films ranges from 0.096 eV to 0.209 eV, which is smaller than the optical band gap values (Section 3.3), indicating the extrinsic conductive mechanism in this temperature region.

3.3. Optical properties

The absorption spectra of the sputtered PbSe thin films were recorded in the infrared region at room temperature. The absorption edge of all the

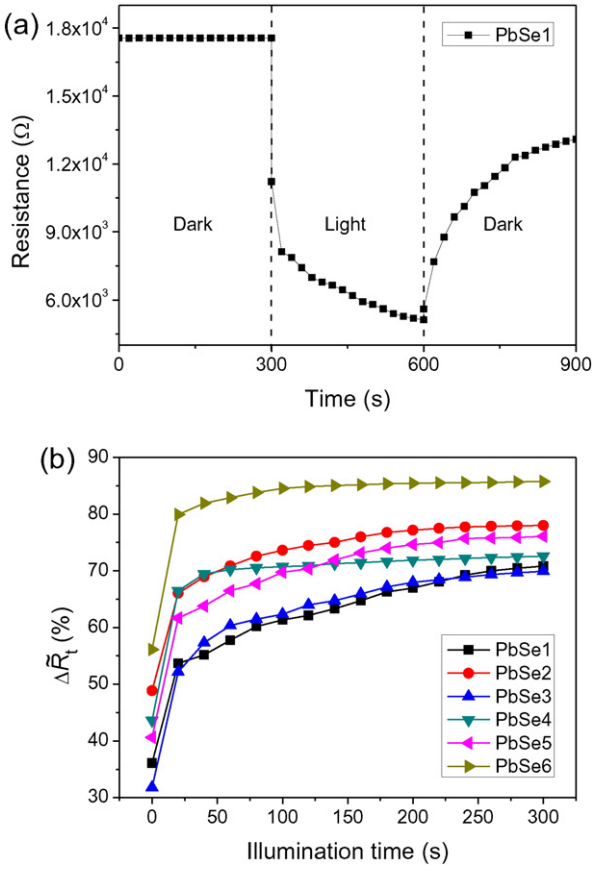

Fig. 2. (a) Resistance variation of the sputtered thin film (PbSe1) in the dark and under certain illumination; (b) resistance change rate under illumination as a function of the illumination time.

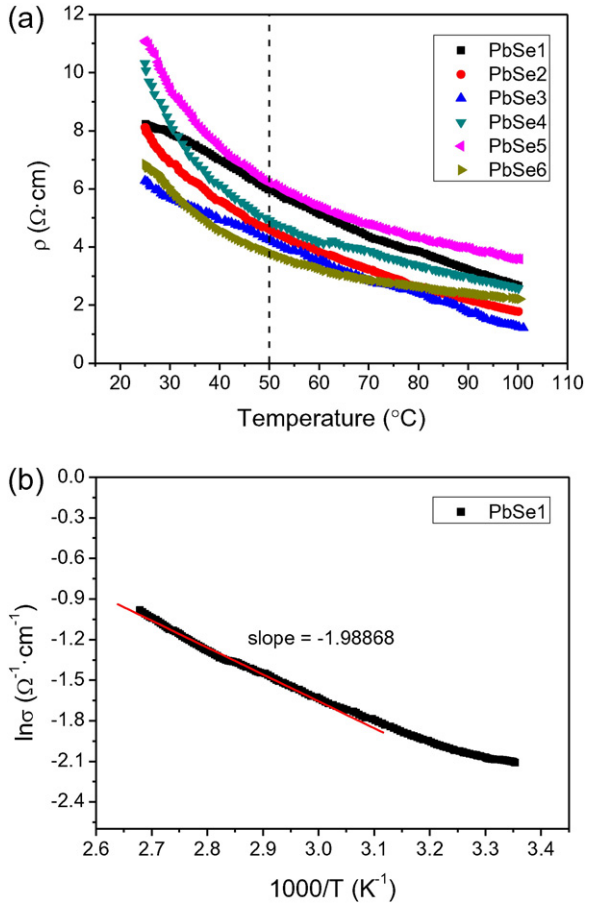

Fig. 3. Electrical properties of the sputtered PbSe thin films: temperature dependence of (a) resistivity and (b) conductivity of the sputtered PbSe thin films.

six sputtered PbSe thin films is located at about 2250 cm^{-1} (4.5 μm), as shown in Fig. 4(a), which is similar to the bulk PbSe materials [31]. Moreover, the strong and sharp peak located at 700 cm^{-1} (14.3 μm) could be due to the phonon absorption from the silicon substrate. Also it is noticed that the absorption of the oxygen impurities in silicon is located at about 1100 cm^{-1}.

The optical properties of the sputtered PbSe thin films can also be evaluated using the optical band gap value, E_g, which is derived from the absorption spectra of these thin films. For semiconductor materials, E_g and the absorption coefficient α obey the Tauc relation [32]:

$$(\alpha h\nu)^{1/n} = B(h\nu - E_g) \tag{3}$$

where α can be derived from the absorption spectrum according to the Lambert–Beer equation applied to solids [26]: $\alpha = 1 / dln(I_0 / I)$, where I_0 is the incident beam intensity and I is the beam intensity after traversing a certain thickness, d, of the sample. $h\nu$ represents the incident beam energy, h is the Planck's constant, and ν is the incident beam frequency ($\nu = 2\pi / \omega$). B is a constant and n is an exponent, which has values of 1/2, 3/2, 2 and 3, depending on the nature of the electronic transition responsible for the absorption: $n = 1/2$ for the allowed direct transition, $n = 3/2$ for the forbidden direct transition, $n = 2$ for the allowed indirect transition and $n = 3$ for the forbidden indirect transition. The electronic transitions of the PbSe thin films obey the role of the direct transition, indicating that $n = 1/2$, so the relation between E_g, α, and the energy of the incident beam $h\nu$ is:

$$(\alpha h\nu)^2 = B(h\nu - E_g). \tag{4}$$

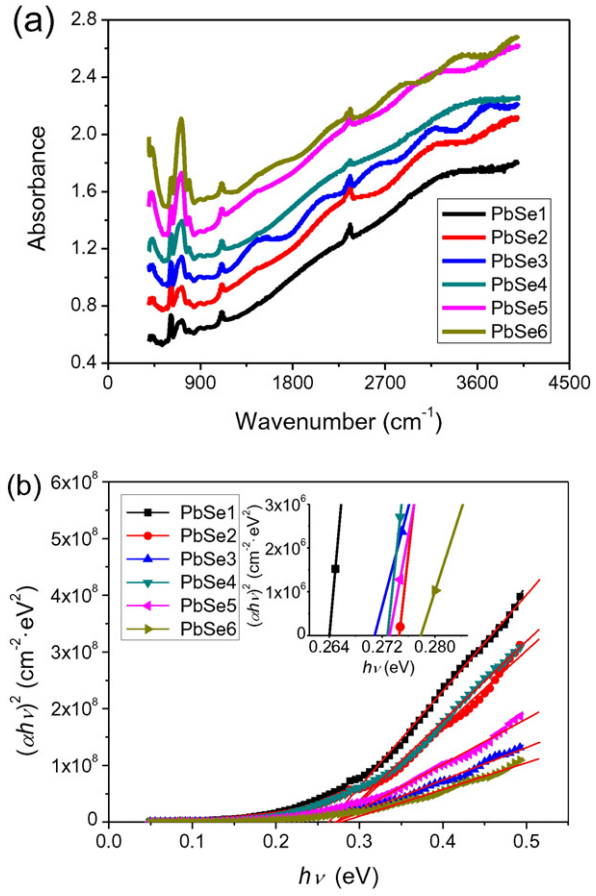

Fig. 4. (a) FT-IR absorption spectra of the sputtered PbSe thin films; (b) relationship between the incident beam energy ($h\nu$) and $(\alpha h\nu)^2$. Inset shows the magnified view of the fitted lines.

Fig. 4(b) presents the variations of $(\alpha h\nu)^2$ with the photon energy, $h\nu$, for the PbSe thin films. The band gap values of the sputtered PbSe films were obtained by extrapolating the linear part of the curve to the incident beam energy axis at $(\alpha h\nu)^2 = 0$, and the results are listed in Table 2. The E_g values of the sputtered PbSe thin films range from 0.264 eV to 0.278 eV, which are similar to the value of the pure bulk PbSe materials ($E_g = 0.28$ eV at 300 K) [15].

3.4. Composition and structure

In order to determine the stoichiometry, the average grain size and crystal structure of the sputtered PbSe thin films, the EDX and XRD analyses were performed. Three elements, Pb, Se and O, were exclusively contained in the sputtered PbSe thin films, according to the EDX results listed in Table 3. The Pb element content is higher than the Se element content, which is contrary to the composition of the PbSe targets. This phenomenon can be explained by the high volatility of Se and the different condensation coefficients for Pb and Se, as mentioned above. One could then expect that in the sputtering process, Se element can be partially lost and the PbSe films will be enriched with Pb and, consequently, will have higher concentrations of the n-type charge carriers than in the initial bulk crystal [27]. Oxygen content shows an erratic dependence on the oxygen flux, although the average content of oxygen in PbSe4, PbSe5 and PbSe6 (1 sccm) is higher than in PbSe1, PbSe2 and PbSe3 (0.5 sccm).

Moreover, the Pb and Se element contents get lower as the O content increases, and the decrease of the Pb element content was lower than the Se element content, according to the slopes of the fit lines, $k_{Pb} = -0.455$, $k_{se} = -0.537$, as shown in Fig. 5. This may be attributed to the Pb–Se bond (302.9 ± 4 kJ mol^{-1}) requiring less energy to be broken than the Pb–O (382.0 ± 12.6 kJ mol^{-1}) and the Se–O (464.8 ± 21.3 kJ mol^{-1}) bond [25]. Thus, the replacement of the Se atoms by the O atoms is much easier than the replacement of the Pb atoms.

Fig. 6 shows the XRD patterns of the sputtered PbSe thin films. Compared with the JCPDS PDF cards, all diffraction peaks belong exclusively to the PbSe phase, which may be attributed to the low content of the oxides and other compounds, confirmed by the XPS results (Section 3.5). The diffraction patterns reveal the rock salt crystal structure of the sputtered PbSe thin films. The peaks at about 29°, 41°, 60° and 97° are attributed to PbSe (200), PbSe (220), PbSe (400) and PbSe (600), respectively. All the PbSe samples exhibit the prominent and intense (200) diffraction peak, indicating that the predominant growth of the crystallites is along the [200] direction. This is due to the lower interface energy along the [200] direction, compared with other crystallographic directions [18].

The average crystal size C_s was calculated using the Debye–Scherrer formula:

$$C_s = \frac{0.9\lambda}{B \cdot \cos\theta} \tag{5}$$

where the 0.9 value is derived from the spherical crystallite geometry, λ denotes the wavelength of the X-ray radiation (Cu Kα, λ = 1.5406 Å), B and θ represent the full width at half maximum (FWHM) and the diffraction angle of the PbSe (200) peak, respectively. The

Table 3
EDX and XRD analytical results of the sputtered PbSe thin films.

Sample	Pb (at.%)	Se (at.%)	O (at.%)	Average crystal size (nm)	Lattice constant (Å)
PbSe1	48.27	44.7	7.03	47.31	6.1655
PbSe2	44.73	44.60	10.67	55.97	6.1684
PbSe3	45.62	44.06	10.32	46.75	6.1645
PbSe4	46.87	41.41	11.72	40.76	6.1626
PbSe5	46.65	43.91	9.44	48.76	6.1684
PbSe6	44.89	41.99	13.12	38.40	6.1615

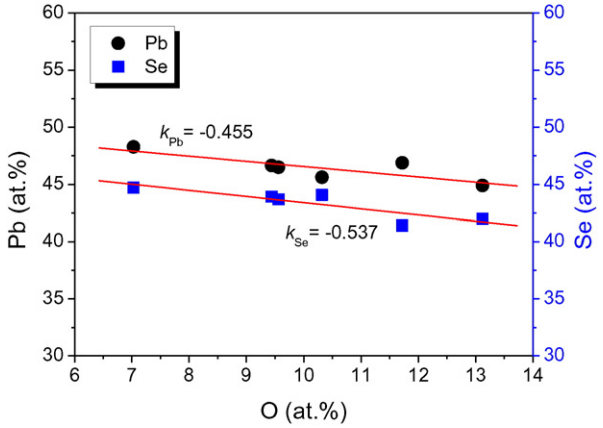

Fig. 5. Pb and Se elements content variations with the O content in the sputtered PbSe thin films.

average crystal size of the sputtered PbSe thin films ranges from 38.4 nm to 55.97 nm. Moreover, the sputtered PbSe thin films with the deposition time of 180 min (PbSe2 and PbSe5) show larger average crystal size than the other four samples, which may be attributed the variation of the internal stress in the thin films during the deposition process [20].

The lattice constant a for the cubic structure was calculated as:

$$a = d\sqrt{h^2 + k^2 + l^2} \tag{6}$$

where d denotes the distance between the atomic lattice planes, and (hkl) are the Miller indices. The lattice constant of the PbSe thin films varies from 6.1615 Å to 6.1684 Å, which is much larger than the bulk material (6.124 Å, JCPDS 06-0354). The deviation of the lattice constant indicates the presence of the lattice strain in the films, which may arise due to the lattice distortion generated by the impurity atoms (most possibly O atoms) during the film formation [33].

3.5. Surface composition

X-ray photoelectron spectroscopy is a surface-sensitive quantitative spectroscopic technique, which measures the relative content, empirical formula, chemical and electronic states of the elements within the sample [34]. Fig. 7 shows the XPS spectra of the Pb4f, Se3d and O1s transitions recorded from the sputtered PbSe thin films.

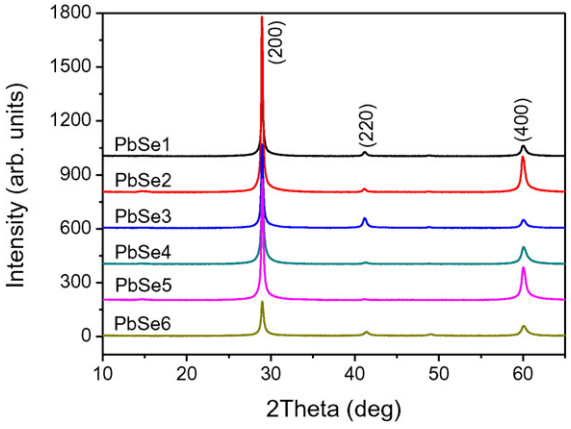

Fig. 6. XRD results of the sputtered PbSe thin films.

The relative content of the elements is calculated using the relative sensitivity factors (RSF) method:

$$\frac{n_i}{n_j} = \frac{I_i/S_i}{I_j/S_j} \tag{7}$$

where n_i/n_j represents the atomic ratio between the element i and j, I_i and I_j denote the peak areas, while S_i and S_j are the RSFs of the two elements. In the present work, the RSFs of the Pb4f, Se3d and O1s are 8.329, 0.853 and 0.78, respectively, and the quantified results are listed in Table 4. The percentage of oxygen is much larger than the results obtained from the EDX test, which may be attributed to the formation of the oxide layer on the surface of the sputtered PbSe thin films, while the thickness of this layer can be analyzed by the etching process discussed later.

In the Pb4f spectra, two transitions are observed with the binding energy of about 137 eV and 142 eV, corresponding to the $Pb4f_{7/2}$ and $Pb4f_{5/2}$ diffraction peaks, respectively, as seen in Fig. 7(a1) and (a2). The Pb4f signal doublet can be fitted with two transitions, and both are ascribed to the Pb^{2+} chemical state. The transitions at around 142.0 eV ($4f_{5/2}$) and 137.1 eV ($4f_{7/2}$) are assigned to the Pb^{2+} in lead selenide (PbSe), and the transitions at around 143.1 eV ($4f_{5/2}$) and 138.0 eV ($4f_{7/2}$) are assigned to the Pb^{2+} in lead oxide (PbO), as seen in Fig. 7(a2). According to these results, the Pb element only has two chemical states, PbSe and PbO, in the sputtered PbSe thin films, and the relative content of these two chemical states is listed in Table 4. Generally, for the Pb element, the content of the PbSe chemical state decreases with the film thickness.

In the Se3d XPS spectra, two transitions with the binding energy of approximately 53 eV and 58 eV are observed, as shown in Fig. 7(b1) and (b2). The fitting results show that three different pairs of transitions, i.e., three different chemical states of the Se element exist in the sputtered PbSe thin films. The transitions at around 53.0 eV ($3d_{5/2}$) and 53.9 eV ($3d_{3/2}$) are assigned to the Se^{2-} in the lead selenide alloy, the transitions at around 54.5 eV ($3d_{5/2}$) and 55.4 eV ($3d_{3/2}$) are assigned to the pure Se element and the transitions at around 58.3 eV ($3d_{5/2}$) and 59.2 eV ($3d_{3/2}$) are assigned to the Se^{4+} in SeO_2, as shown in Fig. 7(b2). The relative content of these three chemical states was calculated the same way as the Pb4f spectra, as listed in Table 4. It can be seen that the content of the PbSe chemical state for the Se element are similar in these six thin films.

In the O1s XPS spectra, two different chemical states of the O element exist in the sputtered PbSe thin films, lattice oxygen and adsorbed oxygen, with the binding energy of about 530.6 eV and 532.1 eV, respectively, as shown in Fig. 7(c1) and (c2). According to the relative content of these two chemical states, as listed in Table 4, more lattice oxygen usually reveals larger $\Delta\tilde{R}$. This can be attributed to the formation of the oxide layer, which functions as a passivation layer on the surface of the PbSe films and, as a result, the surface recombination is reduced significantly [35].

In order to study the surface oxidation of the sputtered PbSe thin films, further XPS analysis after the surface was etched for 60 s by Ar^+ was conducted with the etching power of 3000 eV. Eleven etching and analysis cycles were conducted, and 0 s presents the spectra obtained before the etching treatment, 60 s and 660 s present the first and the eleventh cycles respectively, and the second to the tenth XPS spectra which are similar to the first and the eleventh spectra respectively, were not shown Fig. 8.

The Pb element has two chemical states, PbSe and PbO, before and after the etching treatment, although the content of PbO was reduced after the etching treatment, as shown in Fig. 8(a). The Se element has three chemical states, PbSe, Se and SeO_2, before the films were etched, and two chemical states, Se and SeO_2, disappeared after the etching treatment, as shown in Fig. 8(b), which means that the O atoms contained in the PbSe thin films most probably substitute the Se

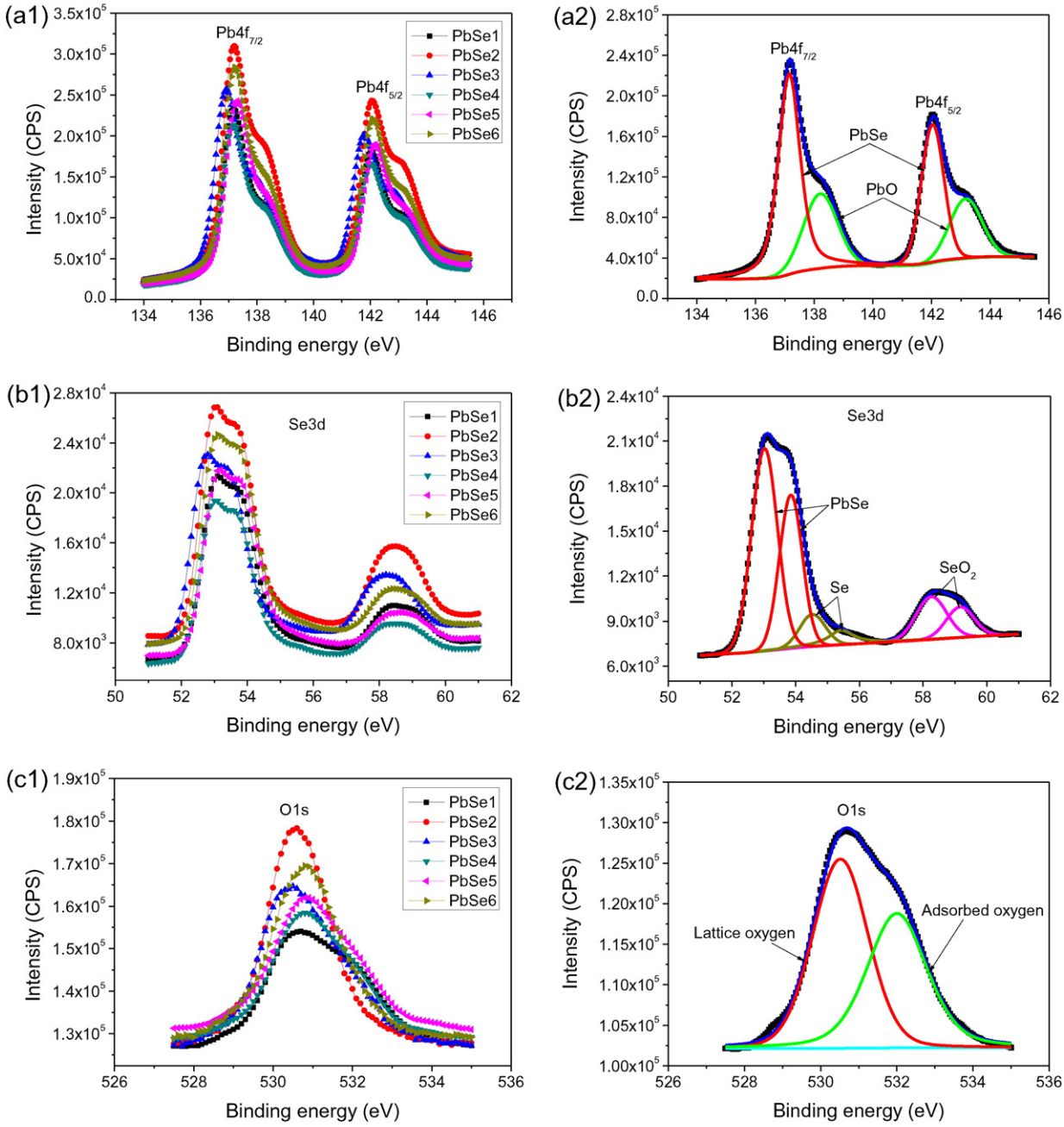

Fig. 7. XPS spectra of the sputtered PbSe thin films: (a1) Pb4f spectra; (a2) analysis result of the Pb4f spectrum recorded in the PbSe1 thin film, other samples are analyzed the same way; (b1) Se3d spectra; (b2) analysis result of the Se3d spectrum recorded in the PbSe1 thin film, other samples are analyzed the same way; (c1) O1s spectra; (c2) analysis result of the O1s spectrum recorded in the PbSe1 thin film, other samples are analyzed the same way.

atoms and bond with the Pb atoms. The adsorbed oxygen chemical state disappeared after the etching treatment conducted for just one cycle, as shown in Fig. 8(c). According to the XPS analysis before and after the etching treatment, there are mainly PbSe and PbO two chemical states in the sputtered PbSe thin films, and within the surface, PbSe, PbO, SeO_2 and adsorbed oxygen, four main chemical states exist. The depth of the etching pit on the sputtered thin films surface is about 110 nm obtained by the profilometer, indicating the etching rate is

Table 4
XPS results of the sputtered PbSe thin films.

Sample	I_{Pb4f}	I_{Se3d}	I_{O1s}	$n_{Pb}:n_{Se}:n_O$	$n_{PbSe}:n_{PbO}$	$n_{PbSe}:n_{Se}:n_{SeO_2}$	$n_{Oabsorbed}:n_{Olttice}$
PbSe1	562,169	32,369	82,422	32:18:50	58:42	71:11:18	46:54
PbSe2	838,225	42,174	105,933	35:17:48	54:46	68:8:24	5:95
PbSe3	684,539	34,584	97,195	33:17:50	38:62	69:9:22	30:70
PbSe4	528,300	27,880	82,556	32:16:52	55:45	73:12:15	31:69
PbSe5	608,243	31,459	85,444	33:17:50	49:51	74:12:14	25:75
PbSe6	718,007	35,879	97,409	34:17:49	47:53	74:11:15	2:98

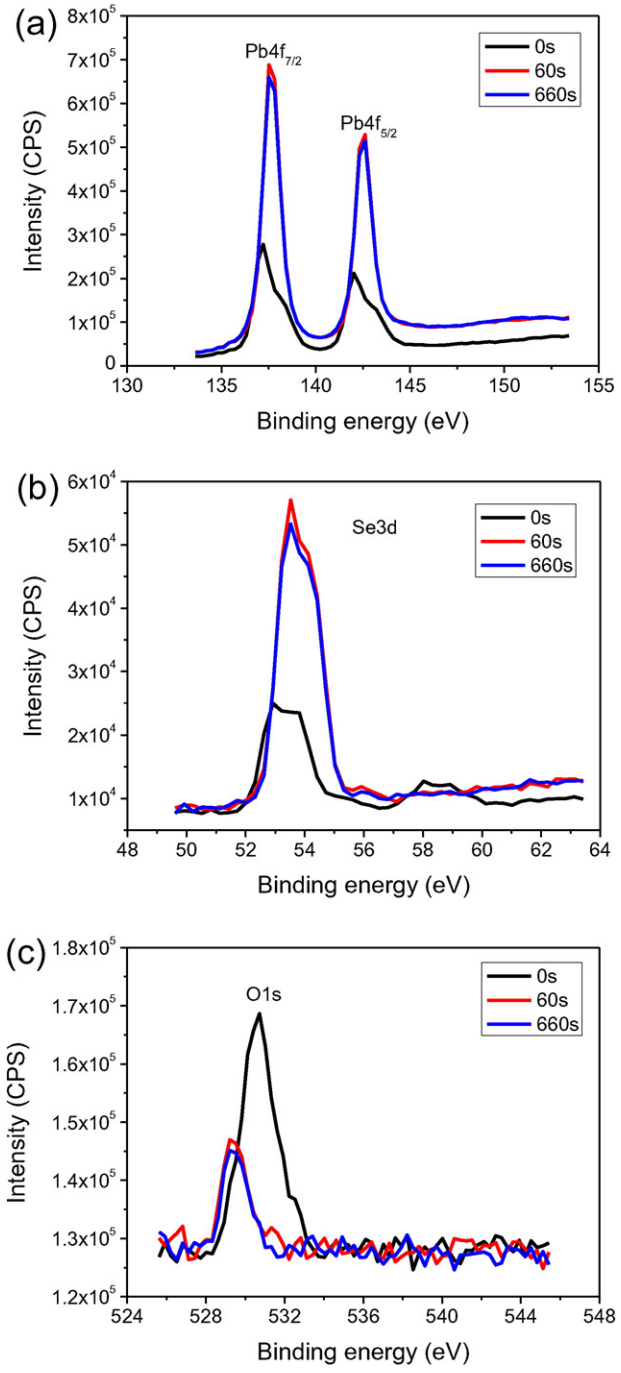

Fig. 8. XPS results of the PbSe thin films before and after the etching treatment: (a) Pb4f spectra; (b) Se3d spectra; (c) O1s spectra.

about 10 nm/min. Combined with the O1s spectra results, one can get that the oxide layer thickness is less than 10 nm.

3.6. Structure and composition effects

As mentioned above, both $\Delta\tilde{R}$ and E_g are very useful parameters to evaluate the photoelectric and optical properties of the thin films, so it is essential to study the effects of the physical and chemical properties of the sputtered PbSe thin films on these two parameters.

Generally speaking, the resistance R of the PbSe thin films can simply be represented as $R = \rho\frac{L}{S}$, here ρ is the resistivity of the thin films, and L and S represent the length and sectional area of the samples, respectively. Thus, according to Eq. (1), $\Delta\tilde{R}$ can be represented as follows:

$$\Delta\tilde{R} = \frac{\rho_D\frac{L}{S} - \rho_L\frac{L}{S}}{\rho_D\frac{L}{S}} \times 100\% \tag{8}$$

where ρ_D and ρ_L is the resistivity of the PbSe samples in the dark and under illumination, respectively. Moreover, $\rho_D = 1/n_D e\mu_D$, $\rho_L = 1/n_L e\mu_L$, where n_D (μ_D) and n_L (μ_L) represent the concentration (mobility) of the charge carriers (electrons and holes) in the dark and under illumination, respectively, and e is the elementary charge. Thus, Eq. (8) can be represented as follows:

$$\Delta\tilde{R} = \frac{\frac{1}{n_D e\mu_D} - \frac{1}{n_L e\mu_L}}{\frac{1}{n_D e\mu_D}} \times 100\%. \tag{9}$$

For a given PbSe sample, the mobility of the charge carriers is hardly varied before and during the illumination treatment if the structure and composition changes in the PbSe thin films were neglected, i.e., $\mu_D \approx \mu_L$. Thus, Eq. (9) can be reduced to:

$$\Delta\tilde{R} = \left(1 - \frac{n_D}{n_L}\right) \times 100\%. \tag{10}$$

Apparently, $\Delta\tilde{R}$ is mainly affected by the ratio between the concentration of the charge carriers in the dark and under illumination. A low carrier concentration in the dark and high carrier concentration under illumination is necessary to obtain high photoelectric sensitivity PbSe thin films.

Generally, the charge carrier concentration is mainly affected by the structure and composition of the thin films. Thus, studying the effects of the structure and composition on the optical and photoelectric properties is useful to prepare high quality PbSe thin films. Within this research, the effects of the structure (mainly the average crystal size and the lattice constant) and composition (mainly the oxygen content and the lattice oxygen percentage) on $\Delta\tilde{R}$ and E_g were studied, as shown in Fig. 9.

As the average crystal size increases from 40.76 nm to 55.97 nm, $\Delta\tilde{R}$ and E_g decrease to a minimum at about 47.31 nm which is approaching the exciton Bohr radius (46 nm) of the bulk PbSe materials, and then increase gradually, as shown in Fig. 9(a). As mentioned in the introduction, the quantum confinement effect is remarkable in the PbSe materials as the grain size is less than their Bohr radius, 46 nm. Thus, when the average crystal size increases from 40.76 nm to 47.31 nm, the quantum confinement effects gradually vanish leading to the decrease of E_g, i.e., the increase of n_D. Besides, the grain boundaries can serve as trap centers and consequently increase the lifetime of the charge carriers, i.e., the concentration of the charge carriers. Thus, the amount of the grain boundaries gradually decreases as the average crystal size increases, leading to the decrease of n_L. Apparently, $\Delta\tilde{R}$ gradually decreases as the average crystal size increases from 40.76 nm to 47.31 nm, according to Eq. (10). When the average crystal size of PbSe thin films is larger than their Bohr radius, the quantum confinement effect is vanished, however, the Columbic attraction between the electron and hole pairs which can decrease E_g, will decrease as the crystal size increases from a critical value, suggested by Lin et al. [36]. Thus, when the average crystal size increases from 47.31 nm to 55.97 nm, E_g gradually increases from the minimum to larger values, which consequently leads to the decrease of n_D. In addition, although the amount

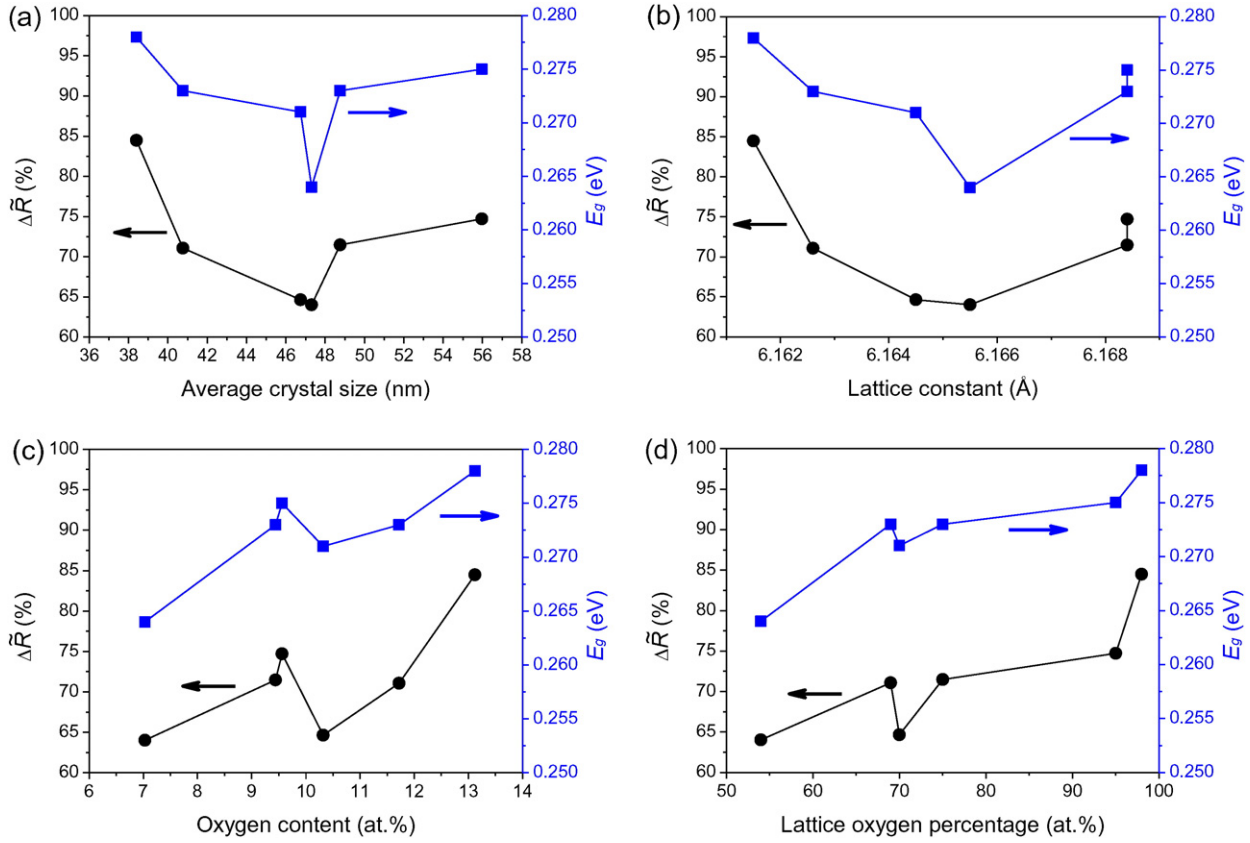

Fig. 9. Resistance change rate under illumination $\Delta\tilde{R}$ and optical band gap E_g variations with: (a) average crystal size, (b) lattice constant, (c) oxygen content and (d) lattice oxygen percentage.

of the grain boundaries gradually decrease, $\Delta\tilde{R}$ still gradually increases with the average crystal size, however, the varying speed is lower than the small average crystal size region (40.76 nm to 47.31 nm), indicating the variation of n_D of is the dominant factor to $\Delta\tilde{R}$ within this region.

$\Delta\tilde{R}$ and E_g show similar variation trends with the lattice constant, which decrease to a minimum and then gradually increase as the lattice constant increases from 6.1615 Å to 6.1684 Å, as shown in Fig. 9(b). It is interesting to notice that the lattice constant roughly increases linearly with the average crystal size, as listed in Table 3, and the 6.1655 Å value which related to the minimum of $\Delta\tilde{R}$ and E_g is corresponding to the average crystal size 47.31 nm which is similar to the Bohr radius of the PbSe material, indicating that the average crystal size is a important factor to the properties of the sputtered PbSe thin films. Generally, the interactions between the atoms gradually decrease as the lattice constant increases, which consequently reduce the degeneracy of the energy levels and result in wider energy band, i.e., narrower band gap [37]. Thus, when the lattice constant increases from 6.1615 Å to 6.1655 Å, n_D gradually increases due to the narrowing band gap. Besides, the reduction of the degeneracy of the energy levels may lead to high recombination rate, i.e., low n_L [38]. Apparently, $\Delta\tilde{R}$ will gradually decrease as the lattice constant increases from 6.1615 Å to 6.1655 Å, according to Eq. (10). However, when the lattice constant increases from 6.1655 Å to 6.1684 Å, the repulsion between the energy levels becomes weak, which consequently push the valence band maximum further down and the conduction band minimum further up, i.e., wide band gap [39]. Thus, when the lattice constant increases from 6.1655 Å to 6.1684 Å, n_D gradually decreases due to the widening band gap. Moreover, the recombination rate of the charge carriers may decrease due to the wide band gap, which consequently results in large n_L. Apparently, $\Delta\tilde{R}$ will gradually increase as the lattice constant increases from 6.1655 Å to 6.1684 Å, according to Eq. (10).

Basically, $\Delta\tilde{R}$ and E_g increase monotonously with the oxygen content, as shown in Fig. 9(c). The chemical states of the oxygen element in the sputtered PbSe thin films include the oxides (mainly PbO), interstitial and substitutional atoms, confirmed by the EDX, XRD and XPS results. Generally, the oxygen atoms diffused into the PbSe crystal lattice can weaken the interaction of the lattice atoms and inhibit the motion of the delocalized electrons, which consequently result in a wider band gap and lower n_D as the oxygen content increases [27]. Besides, the oxygen chemical states can act as the trap centers which can quite extend the lifetime of the charge carriers, and consequently increase the concentration of the charge carriers, i.e., larger n_L [35]. Thus, $\Delta\tilde{R}$ and E_g increase monotonously with the oxygen content.

The variations of $\Delta\tilde{R}$ and E_g with the lattice oxygen percentage in the sputtered PbSe thin films also increase monotonously, as shown in Fig. 9(d), which can be explained by the sensitization theory [40,41]. The surface oxidation can enhance the photoelectric sensitivity of the PbSe thin films since the oxide layer can act as a passivation layer which can trap the charge carriers and increase their concentration, i.e., large n_L. On the other hand, the oxide layer can inhibit the transition of the charge carriers, leading to a wider band gap, which consequently result in lower n_D. Thus, $\Delta\tilde{R}$ and E_g increase monotonously with the lattice oxygen percentage.

In summary, the variation trends of $\Delta\tilde{R}$ and E_g with the average crystal size, lattice constant, oxygen content and lattice oxygen percentage are similar, respectively.

These four parameters generate different effects on the concentration of the charge carriers, which consequently affect the photoelectric and optical properties of the sputtered PbSe thin films. Moreover, both controlling the deviation of the average crystal size from the Bohr radius and increasing the oxygen content are direct and effective ways to obtain high photoelectric sensitivity PbSe thin films.

4. Conclusions

The PbSe thin films were grown on Si (111) substrates under different deposition times and oxygen fluxes using magnetron sputtering, and the film structure and composition effects on their photoelectric and optical properties were studied. The optical band gaps of all six sputtered PbSe thin films ranged from 0.264 eV to 0.278 eV, which are similar to the bulk PbSe materials (0.28 eV at 300 K). In addition, the PbSe thin film prepared with oxygen flux 1.0 sccm, deposition time 240 min sputtering power 150 W and substrate temperature 150 °C showed the highest resistance change rate under illumination, about 84.47%. The variation trends of the resistance change rate under illumination and the optical band gap with the average crystal size, lattice constant, oxygen content and lattice oxygen percentage were similar, respectively. The sputtered PbSe thin films showed poor photoelectric sensitivity, when the average crystal size was similar to the Bohr radius (46 nm), while the photoelectric sensitivity increased with the oxygen content in the thin films, indicating both controlling the deviation of the average crystal size from the Bohr radius and increasing the oxygen content are two direct and effective ways to obtain high photoelectric sensitivity PbSe thin films.

Acknowledgments

This work was supported by the National Nature Science Foundation of China (51271022) and the Fok Ying Tung Education Foundation (132001).

References

[1] F. Braun, Ueber die Stromleitung durch Schwefelmetalle ("On current flow through metallic sulfides"), Ann. Phys. Chem. 153 (1874) 556–563.
[2] W.J. Hu, S. Gao, P.N. Prasad, J.K. Wang, J. Xu, Employing photoassisted ligand exchange technique in layered quantum dot LEDs, J. Nanomater. 2012 (2012) 183–190.
[3] H. Preier, Recent advances in lead-chalcognide diode lasers, Appl. Phys. 20 (1979) 189–206.
[4] J.M. Martin, J.L. Hernández, L. Adell, A. Rodriguez, F. López, Arrays of thermally evaporated PbSe infrared photodetectors deposited on Si substrates operating at room temperature, Semicond. Sci. Technol. 11 (1996) 1740–1744.
[5] J.J. Choi, Y.F. Lim, M.B. Santiago-Berrios, M. Oh, B.R. Hyun, L.F. Sun, A.C. Bartnik, A. Goedhart, G.G. Malliaras, H.D. Abruña, F.W. Wise, T. Hanrath, PbSe nanocrystal excitonic solar cells, Nano Lett. 9 (2009) 3749–3755.
[6] J.P. Heremans, V. Jovovic, E.S. Toberer, A. Saramat, K. Kurosaki, A. Charoenphakdee, S. Yamanaka, G.J. Snyder, Enhancement of thermoelectric efficiency in PbTe by distortion of the electronic density of states, Science 321 (2008) 554–557.
[7] A. Krier, Mid-infrared Semiconductor Optoelectronics (Springer Series in Optical Sciences), Springer London Ltd., 2006
[8] S. Mukherjee, D.H. Li, A. Gautam, J.P. Kar, Z.S. Shi, Lead Salt Thin Film Semiconductors for Microelectronic Applications, Transworld Research Network, 2010 1–88.
[9] W.L. Ma, J.M. Luther, H.M. Zheng, Y. Wu, A.P. Alivisatos, Photovoltaic devices employing ternary PbS_xSe_{1-x} nanocrystals, Nano Lett. 9 (2009) 1699–1703.
[10] G. Springholz, V. Holy, M. Pinczolits, G. Bauer, Self-organized growth of three-dimensional quantum-dot crystals with fcc-like stacking and a tunable lattice constant, Science 282 (1998) 734–737.
[11] M.A. Alvi, Z.H. Khan, Synthesis and characterization of nanoparticle thin films of a-$(PbSe)_{100-x}Cd_x$ lead chalcogenides, Nanoscale Res. Lett. 8 (2013) 148.
[12] W.A. Tisdale, K.J. Williams, B.A. Timp, D.J. Norris, E.S. Aydil, X.Y. Zhu, Hot-electron transfer from semiconductor nanocrystals, Science 328 (2010) 1543–1547.
[13] Y. Liu, M. Gibbs, J. Puthussery, S. Gaik, R. Ihly, H.W. Hillhouse, M. Law, Dependence of carrier mobility on nanocrystal size and ligand length in PbSe nanocrystal solids, Nano Lett. 10 (2010) 1960–1969.
[14] S. Abe, One-step synthesis of PbSe–ZnSe composite thin film, Nanoscale Res. Lett. 6 (2011) 324.
[15] E.B. Salgado, M.T.S. Nair, P.K. Nair, R.A. Zingaro, Chemically deposited thin films of PbSe as an absorber component in solar cell structures, Thin Solid Films 519 (2011) 7432–7437.
[16] N. Mukherjee, A. Mondal, Comparative study on the properties of galvanically deposited nano- and microcrystalline thin films of PbSe, J. Electron. Mater. 39 (2010) 1177–1185.
[17] S. Gad, M.A. Rafea, Y. Badr, Optical and photoconductive properties of $Pb_{0.9}Sn_{0.1}Se$ nano-structured thin films deposited by thermal vacuum evaporation and pulsed laser deposition, J. Alloys Compd. 515 (2012) 101–107.
[18] A.D.R. Pillai, K. Zhang, K. Bollenbach, D. Nminibapiel, W. Cao, H. Baumgart, V.S.K. Chakravadhanula, C. Kübel, V. Kochergin, ALD growth of PbTe and PbSe superlattices for thermoelectric applications, ECS Trans. 58 (10) (2013) 131–139.
[19] X.J. Wang, Y.B. Hou, Y. Chang, C.R. Becker, R.F. Klie, R. Kodama, F. Aqariden, S. Sivananthan, Growth of PbSe on ZnTe/GaAs(211)B by molecular beam epitaxy, J. Cryst. Growth 312 (2010) 910–913.
[20] H. Jung, R. Kuljic, M.A. Stroscio, M. Dutta, Confinement in PbSe wires grown by rf magnetron sputtering, Appl. Phys. Lett. 96 (2010) 153106.
[21] M. Fardy, A.I. Hochbaum, J. Goldberger, M.J. Zhang, P.D. Yang, Synthesis and thermoelectrical characterization of lead chalcogenide nanowires, Adv. Mater. 19 (2007) 3047–3051.
[22] K.R. Murali, P. Ramanathan, Characteristics of slurry coated lead selenide films, Chalcogenide Lett. 6 (2009) 91–95.
[23] Z.W. Quan, Z.P. Luo, W.S. Loc, J. Zhang, Y.X. Wang, K.K. Yang, N. Porter, J. Lin, H. Wang, J.Y. Fang, Synthesis of PbSeTe single ternary alloy and core/shell heterostructured nanocubes, J. Am. Chem. Soc. 133 (2011) 17590–17593.
[24] M.A. Barote, A.A. Yadav, R.V. Surywanshi, L.P. Deshmukh, E.U. Masumdar, Chemical bath deposited PbSe thin films: optical and electrical transport properties, Res. J. Chem. Sci. 2 (2012) 15–19.
[25] C. Gautier, M. Cambon-Muller, M. Averous, Study of PbSe layer oxidation and oxide dissolution, Appl. Surf. Sci. 141 (1999) 157–163.
[26] V. Arivazhagan, M. Manonmani Parvathi, S. Rajesh, Impact of thickness on vacuum deposited PbSe thin films, Vacuum 86 (2012) 1092–1096.
[27] E.I. Rogacheva, T.V. Tavrina, S.N. Grigorov, O.N. Nashchekina, V.V. Volobuev, A.G. Fedorov, K.A. Nasedkin, M.S. Dresselhaus, Effect of oxidation on the thermoelectric properties of PbSe thin films, J. Electron. Mater. 4 (2003) 298–303.
[28] X.G. Sun, K.W. Gao, X.L. Pang, H.S. Yang, A.A. Volinsky, Thickness effect on the band gap of magnetron sputtered $Pb_{45}Se_{45}O_{10}$ thin films on Si, Phys. E. 67 (2015) 152–158.
[29] D.H. Yu, C.Y. Wang, X.L. Cheng, Y.X. Song, Recent development of magnetron sputtering processes, Vacuum 46 (2009) 19–25.
[30] S.D. Delekar, M.K. Patil, B.V. Jadhav, K.R. Sanadi, P.P. Hankare, Synthesis and characterization of $Cd_{0.7}Pb_{0.3}Se$ thin films for photoelectrochemical solar cell, Sol. Energy 84 (2010) 394–400.
[31] P.A. Loiko, G.E. Rachkovskaya, G.B. Zacharevich, V.S. Gurin, M.S. Gaponenko, K.V. Yumashev, Optical properties of novel PbS and PbSe quantum-dot-doped alumino-alkali-silicate glasses, J. Non-Cryst. Solids 358 (2012) 1840–1845.
[32] A.A. Al-Ghamdi, S. Al-Heniti, S.A. Khan, Structural, optical and electrical characterization of Ag doped lead chalcogenide (PbSe) thin films, J. Lumin. 135 (2013) 295–300.
[33] A. Begum, A. Hussain, A. Rahman, Effect of deposition temperature on the structural and optical properties of chemically prepared nanocrystalline lead selenide thin films, Beilstein J. Nanotechnol. 3 (2012) 438–443.
[34] Y. Zhou, G.H. Wu, Analysis Methods in Materials Science-X-ray Diffraction and Electron Microscopy in Materials Science, second ed. Harbin Institute of Technology Press, Harbin, 2011.
[35] F. Zhao, S. Mukherjee, J. Ma, D. Li, S.L. Elizondo, Z. Shi, Influence of oxygen passivation on optical properties of PbSe thin films, Appl. Phys. Lett. 92 (2008) (211110–211110–3).
[36] H. Lin, C.P. Huang, W. Li, C. Ni, S.I. Shah, Y.H. Tseng, Size dependency of nanocrystalline TiO_2 on its optical property and photocatalytic reactivity exemplified by 2-chlorophenol, Appl. Catal. B Environ. 68 (2006) 1–11.
[37] S.V. Streltsov, A.Y. Manakov, A.P. Vokhmyanin, S.V. Ovsyannikov, V.V. Shchennikov, Crystal lattice and band structure of the intermediate high-pressure phase of PbSe, J. Phys. Condens. Matter 21 (2009) 385501.
[38] S.H. Wei, A.L. Zunger, Electronic and structural anomalies in lead chalcogenides, Phys. Rev. B 1 (1997) 13605.
[39] K.K. Zhuravlev, PbSe vs. CdSe: Thermody namic properties and pressure dependence of the band gap, Physica B 394 (2007) 1–7.
[40] Q. Wu, P. Li, The effect of grain boundaries barrier in PbS polycrystalline film applied to photoconduction, Acta Phys. Sin. 18 (1962) 259–263.
[41] F.H. Zhao, J.G. Ma, D.H. Li, S. Mukherjee, G. Bi, Z.S. Shi, Influence of oxygen post-growth annealing on optical and electrical properties of PbSe thin films, J. Electron. Mater. 38 (2009) 1661–1665.